

Article

Effect of Two-Step High Temperature Treatment on Phase Transformation and Microstructure of V-Bearing Bainitic Steel

Bo Lv ¹, Dongxin Yin ², Dongyun Sun ², Zhinan Yang ², Xiaoyan Long ^{2,3,*} and Zeliang Liu ³

¹ School of Environmental and Chemical Engineering, Yanshan University, Qinhuangdao 066004, China; longxiaoyanlx@163.com

² State Key Laboratory of Metastable Materials Science and Technology, Yanshan University, Qinhuangdao 066004, China; 2817248300@163.com (D.Y.); w11661493@163.com (D.S.); lyn3640@163.com (Z.Y.)

³ Key Laboratory of Mechanical Reliability for Heavy Equipments and Large Structures of Hebei Province, Yanshan University, Qinhuangdao 066004, China; liuzeliang@ysu.edu.cn

* Correspondence: longxy2021@126.com

Abstract: The effects of VC precipitation on phase transformation, microstructure, and mechanical properties were studied by controlling two-step isothermal treatment, i.e., austenization followed by intercritical transformation. The results show that the bainite transformation time of 950 °C–860 °C treatment and 950 °C–848 °C treatment is shorter than that of 950 °C single-step treatment. This is related to the isothermal ferrite transformation in the intercritical transformation range. The formation of ferrite nuclei increases the density of medium temperature bainite nucleation sites and decrease the bainite nucleation activation energy. At the same time, a large number of VC particles are precipitated. The additional VC particles provide numbers of preferential nucleation sites. The toughness of the specimen treated at 950–870 °C is improved, which is related to the large proportion of high angle grain boundaries. High angle grain boundaries can hinder crack propagation or change the direction of crack propagation. The specimen treated at 950 °C–848 °C exhibits large proportion of low angle grain boundaries, which is beneficial for the strength improvement.

Keywords: VC precipitation; two-step isothermal process; bainitic transformation



Citation: Lv, B.; Yin, D.; Sun, D.; Yang, Z.; Long, X.; Liu, Z. Effect of Two-Step High Temperature Treatment on Phase Transformation and Microstructure of V-Bearing Bainitic Steel. *Metals* **2022**, *12*, 983. <https://doi.org/10.3390/met12060983>

Academic Editor: João Pedro Oliveira

Received: 27 April 2022

Accepted: 2 June 2022

Published: 7 June 2022

Publisher's Note: MDPI stays neutral with regard to jurisdictional claims in published maps and institutional affiliations.



Copyright: © 2022 by the authors. Licensee MDPI, Basel, Switzerland. This article is an open access article distributed under the terms and conditions of the Creative Commons Attribution (CC BY) license (<https://creativecommons.org/licenses/by/4.0/>).

1. Introduction

Carbide-free bainitic was obtained in Si/Al-bearing steel, the Si/Al elements effectively prevent carbide precipitation in bainitic transformation. It has been widely used in wear resistance steel plate, bearing, and frog due to its high strength, toughness, wear resistance, and fatigue resistance [1–3]. Bainite transformation often requires a long-time isothermal transformation; improving its production efficiency is one of the urgent problems to be solved. Numerous methods, such as adding alloy elements (e.g., Al and Co) [4,5], controlling the second phase to increase the nucleation sites [6,7], and pre-forming ferrite or martensite [8,9], have been used to accelerate the bainite transformation.

Vanadium was discovered by the Swedish scientist and doctor Nils Gabriel Sefström in 1830. However, the work of Sefström and the famous Swedish chemist Jöns Jacob Berzelius was confined to chemical studies of a large number of vanadium compounds. It was only some 30 years later that vanadium was isolated as a metal due to work by the English chemist, Sir Henry Roscoe [10]. Vanadium is a strong carbide and nitride forming element [11,12]. The amount of precipitated V is temperature dependent. The fine VC or V (C, N) precipitation are mainly formed during and after the transformation of austenite to ferrite. The lattice misfit of V (C, N) and ferrite is low, precipitation of V (C, N) can serve as the preferred sites for the nucleation of acicular ferrite, promoting intragranular ferrite transformation and refining the ferrite grain [13]. V (C, N) precipitations preferentially precipitate in the semi-coherent manner of low-index close surfaces, which can make misfit of dislocations as small as possible. Thereby, the interface energy of V (C, N)

precipitations and bainite nuclei are decreased, accelerating the bainite transformation [14]. The precipitation volume of V (C, N) in bainitic transformation region increases with the increase of temperature. The latest research [15] indicates that the introduction of fine VC precipitation during bainitic austempering can significantly accelerate the bainite transformation, reducing the incubation period by 91%. The reduction of the activation energy of bainite nucleation and the generation of preferential nucleation sites at the vanadium carbide/austenite interface facilitate the acceleration of bainite formation kinetics. In addition, the introduction of VC in the bay region can simultaneously improve the tensile strength and impact toughness of steels.

The precipitations of V play a role in precipitation strengthening and grain refinement strengthening in steel [16]. The research of Nafisi's team has shown that fine VC particles formed by adding 0.06 wt% V could increase yield and tensile strength of 60–95 MPa without losing toughness and ductility [17]. Wang found [18] that the addition of V can widen the bainite phase region during continuous cooling. Furthermore, the addition of fine VC precipitations with a mass fraction of 0.06% can increase the yield strength and tensile strength by 60 MPa and 95 MPa, respectively, without decreasing the toughness and ductility [19]. Karmakar's team prepared two V-containing steels, high C with low N and low C with high N. At moderate isothermal holding temperatures (600–650 °C), the largest amount of fine V (C, N) precipitated phase was found in both steels. The V precipitations of the low C with high N steel are finer, which can offset the strength reduction caused by unfavorable factors such as microstructure coarsening [19]. It is shown that V (C, N) precipitation makes dislocation entanglement recovery difficult [20]. V-containing steels have a high proportion of low- and medium-angle grain boundaries and a small bainite grain size [21]. Garmeh et al. showed that the addition of vanadium to silicon-containing medium carbon steel is helpful to the formation of carbide-free bainitic ferrite. At the same time, the addition of vanadium increases the grain size of primary austenite and the content of retained austenite. In the process of transformation induced plasticity, retained austenite transforms into martensite, which leads to the improvement of tensile strength and fracture toughness [22]. The introduction of V microalloying in bainitic steels has a positive effect on strength. Therefore, it is important to study the effect of V precipitations on the bainite transformation and the relationship between the microstructure and mechanical properties.

In this study, V microalloying is introduced on the basis of medium carbon bainitic steel. Precipitations of V with different contents are introduced before the bainite austempering. The accelerated bainite transformation mechanism is studied by controlling the number of V precipitations. The volume fraction of bainitic ferrite and retained austenite by a high-temperature two-stage isothermal process, and its influence on the microstructure and mechanical properties of the tested steel is explored.

2. Tested Material and Methods

Tested steel: The steel used in this study is a V microalloyed medium carbon bainitic steel, and its specific chemical compositions Fe-0.40C-1.53Mn-1.53Si-1.09Cr-0.31Mo-0.15V (wt.%). The weight of 50 kg ingot was smelted by vacuum melting furnace. After homogenization, the ingot was hot-forged into a rectangular with a cross-section of 60 × 60 mm².

Points of phase transformation: The phase transition point of the tested steel was measured by the DIL 805 A/D dilatometer. Figure 1 is the expansion curve of the sample during continuous heating. A_{c1} is the start temperature of austenite transformation, and A_{c3} is the finish temperature of austenite transformation. The transformation point A_{c1} of the tested steel measured by the tangent method is 731 °C, and the A_{c3} is 864 °C. The specimens were heated to 950 °C at a heating rate of 10 °C/s using a DIL 805 A/D dilatometer and held for 30 min, then rapidly cooled to 890 °C, 870 °C, 860 °C, and 848 °C, respectively, for 30 min in a vacuum with 30 °C/s. After that, the specimens were cooled to room temperature at a cooling rate of 30 °C/s. Finally, after the M_s of the test steel was determined, a bainitic austempering temperature of 320 °C was selected.

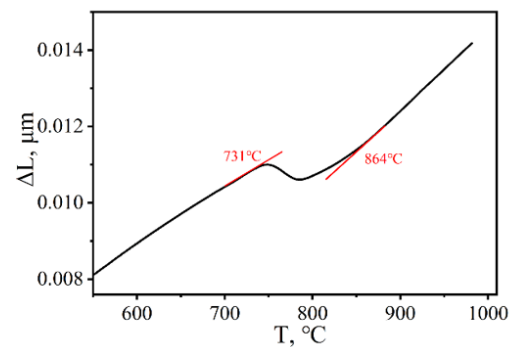


Figure 1. Thermal expansion curve.

Heat treatment process: The high-temperature two-stage isothermal heat treatment of the tested steel was designed, as shown in Figure 2. All samples were homogenized and annealed at 1050 $^{\circ}\text{C}$ for 3 h, ensuring that V was completely dissolved in the matrix. The martensite microstructure was formed by oil quenching. Then, the specimens were reheated to 950 $^{\circ}\text{C}$ for 30 min, followed by rapid cooling to 890 $^{\circ}\text{C}$, 870 $^{\circ}\text{C}$, 860 $^{\circ}\text{C}$, and 848, respectively, $^{\circ}\text{C}$ for 30 min. After that, the specimens were austempered at 320 $^{\circ}\text{C}$ for 2 h in a salt bath furnace for bainitic transformation.

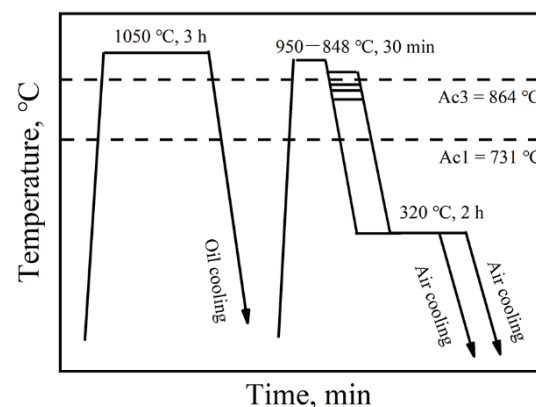


Figure 2. Schematic diagram of heat treatment process.

Microstructure and properties characterization: Scanning electron microscope (SEM) of Hitachi Tokyo Japan and transmission electron microscope (TEM) of Thermo Fisher, Waltham, MA, USA, was used to investigate the microstructures of the tested steels. The surface of specimens after mechanical polishing was electropolished by employing an electropolisher (ElectroMet 4), for EBSD of EDAX, Warrendale, PA, USA, analysis. The employed electrolyte consisted of perchloric acid with a concentration of approximately 10% and absolute ethyl alcohol with a content of approximately 90% in experiment of EBSD Electrolytic polishing. The voltage, electric current, and time for the electropolishing process were approximately 30 V, 1.8 A, and 15 s, respectively. The scanning step was 30 nm for EBSD data collection. The volume fraction of the retained austenite was measured by X-ray diffraction (XRD). In addition, an MTS tensile testing machine was used to gain the mechanical properties of the prepared steels at a constant tensile speed of 3 mm/min. The parallel section of the tensile specimen was a round bar with a diameter of 5 mm and gauge length of 25 mm. The JB-300 pendulum impact tester was employed to conduct a room temperature impact tests on the steels. The dimension of specimen is 10 mm \times 10 mm \times 55 mm with a U notch and its root radius is 1 mm. Three specimens were prepared for each group of experiments and the average value was used to determine the experimental results. The hardness test was carried out by using HR-150A, Rockwell hardness tester with a load capacity of 150 kg.

3. Results

3.1. Precipitation Kinetic Simulation of VC

Simulation for VC precipitates during the holding were performed with DICTRA™ module of the Thermo-Calc® software, 2020b, Stockholm, Sweden using the TCFE11 and MOBFE6 databases. The equilibrium phase diagram module of the Thermo–Calc software is used to simulate the V component in the Austenite phase with the increase of the Austenite temperature. Figure 3a shows the variation of the mass percentage of V in austenite phase with the increase of austenitizing temperature. This demonstrates the variation of V dissolved in the matrix with increasing austenitization temperature. The results show that the dissolution of V in the matrix increases with the increase of austenitization temperature. All VC precipitations dissolve into the austenite when the temperature reaches around 970 °C. Figure 3b shows the variation of VC volume fraction with holding temperature and holding time. It can be seen that the volume fraction of VC precipitations is related to the holding temperature and holding time. The rate of VC precipitation shows a rapid and then slow tendency with the increase of time. The change of VC volume fraction in all processes tends to be stable after 30 min. The volume fraction of precipitated VC gradually decreases as the isothermal temperature gradually increases from 800 °C to 890 °C. When the temperature is kept at 890 °C for 30 min, the volume fraction of precipitated VC is almost 0, as shown in Figure 3c.

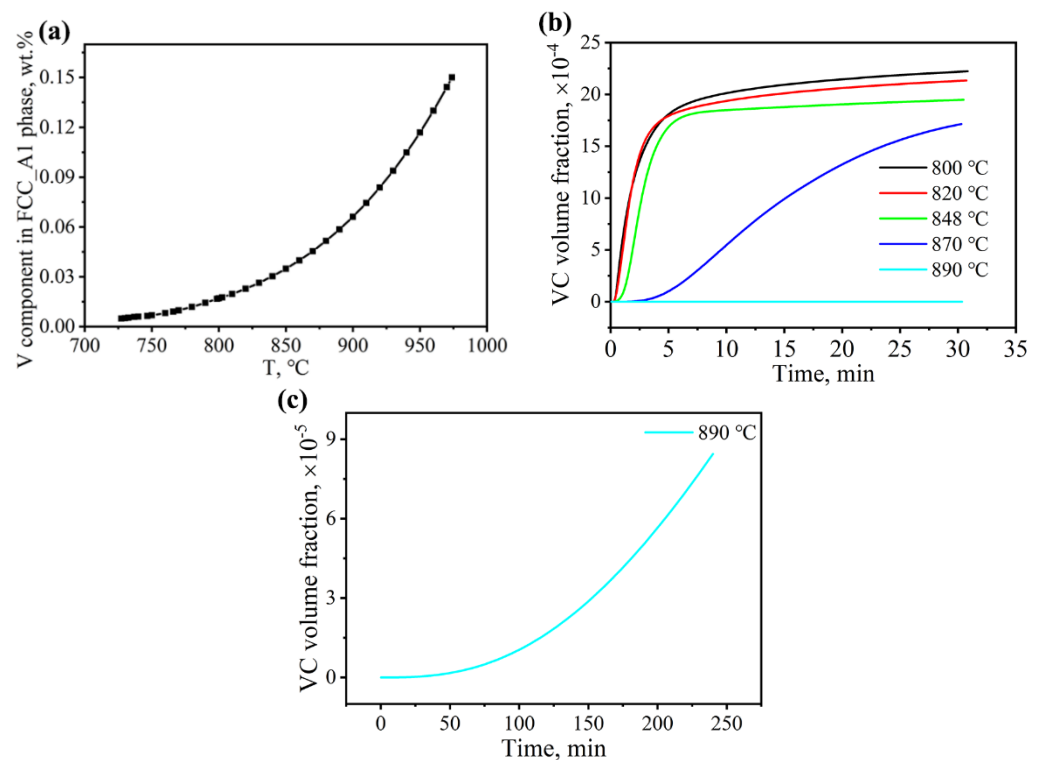


Figure 3. (a) V component in the austenite phase with the increase of the austenitization temperature; (b) and (c) Relationship between VC volume fraction and time.

When there is a free energy difference between the V precipitation and the parent phase, a phase transformation driving force will be generated, followed by forming V precipitation. According to the VC solid solubility product formula, the free energy formula of VC precipitated phase transition can be obtained [23]:

$$\text{Lg}([\text{V}] \cdot [\text{C}]) = -9500/T \quad (1)$$

$$\begin{aligned}\Delta G_p^\theta &= \ln 10 \cdot (A - B/T) - \ln 10 \cdot RT \cdot \log (\prod [M]^{V_i}) \\ &= -19.1446B + 19.1446T \{A - \log (\prod [M]^{V_i})\}\end{aligned}\quad (2)$$

$$\begin{aligned}G_{VC}^\theta &= -19.1446B + 19.1446T \{A - \log (\prod [M]^{V_i})\} \\ &= -19.1446 \times 9500 + 19.1446T \{6.72 - \log (0.40 \times 0.15)\} \\ &= -181,873.77 + 152.04T\end{aligned}\quad (3)$$

where, ΔG_{VC}^θ is VC precipitated phase free energy difference (J/mol); [M] is element content dissolved in the matrix (wt.%); A and B are constant in the formula of VC solid solubility product; and T is absolute temperature. After calculation, the free energy difference between VC and matrix is -5051 J/mol at 890°C . The larger the free energy difference, the easier the VC precipitation.

3.2. Dynamics of Bainite Transformation

The M_s of the tested steel is measured by a DIL805 A/D dilatometer. Figure 4 shows the expansion–temperature curves of the tested steel at different isothermal treatment. Figure 4b is an enlarged figure of Figure 4a located at the transformation point. As shown in Figure 4b, the change of the M_s is small. This means that adding the second-stage high temperature heat treatment has little effect on the partitioning of element C. Therefore, the effect of alloying elements on bainite phase transformation at 320°C is almost uniform in different specimens.

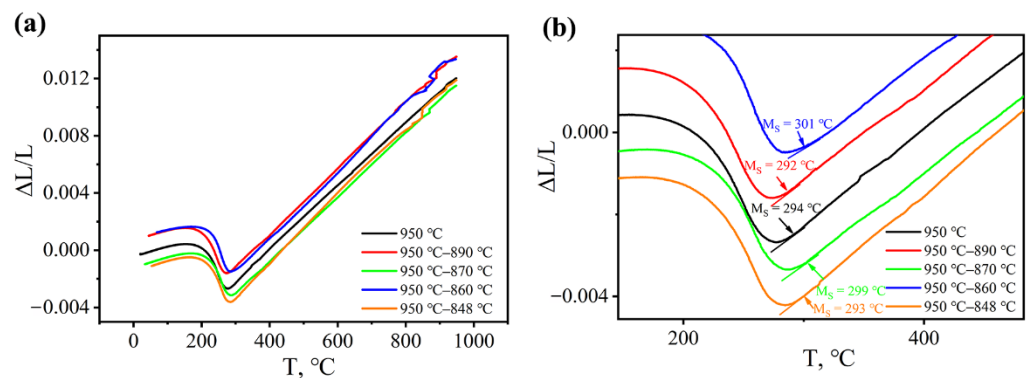


Figure 4. (a) Temperature–expansion curves at different austenitization temperatures; (b) Enlarged figure of (a) located at the transformation point.

The specimens were heated to 950°C at a heating rate of 10 C/s using a DIL 805 A/D dilatometer and held for 30 min. Then rapidly cooled to 890 , 870 , 860 , and 848°C , respectively, for 30 min in a vacuum with 30°C/s . After that, the specimens were cooled to 320°C at a with 30°C/s to carry out isothermal transformation of bainite. The bainite transformation kinetic curves of different specimens at 320°C are shown in Figure 5. Figure 5b is the magnification of the black circle part of the time–expansion curve of Figure 5a at different temperatures. It shows the change of the expansion amount at different austenitizing temperatures. It can be observed that when the austenitization temperature decreased from 890°C to 848°C , the expansion of the specimen gradually increased, from $0.800\ \mu\text{m}$ to $1.146\ \mu\text{m}$. This phenomenon is caused by the amount of VC precipitations. The curves have some fluctuations at the beginning of the second stage of the isothermal treatment, which is caused by the temperature instability during the cooling process of the dilatometer. Curves in Figure 5c show the bainite isothermal transformation kinetics of different specimens. The bainite is completely transformed in about 2 h. The incubation period of different specimens is very short, about 30 s. Figure 5d shows the bainite transformation rate of the different specimens. It can be seen that the bainite transformation rates of the specimens with different heat treatment increased and then decreased with time, and the peak transformation rates were different.

Compared with 950 °C single-stage treatment, the peak of bainite transformation shifted to the right and the bainite transformation time increased for 950 °C–890 °C and 950 °C–870 °C treatments; the peak of bainite transformation shifted to the left and the bainite transformation time decreased for 950 °C–860 °C and 950 °C–848 °C treatments. This indicates that the isothermal temperature in the second stage has an effect on the bainite transformation. The low temperature in the second stage favors bainite transformation, while the high temperature in the second stage is not conducive to the bainite transformation.

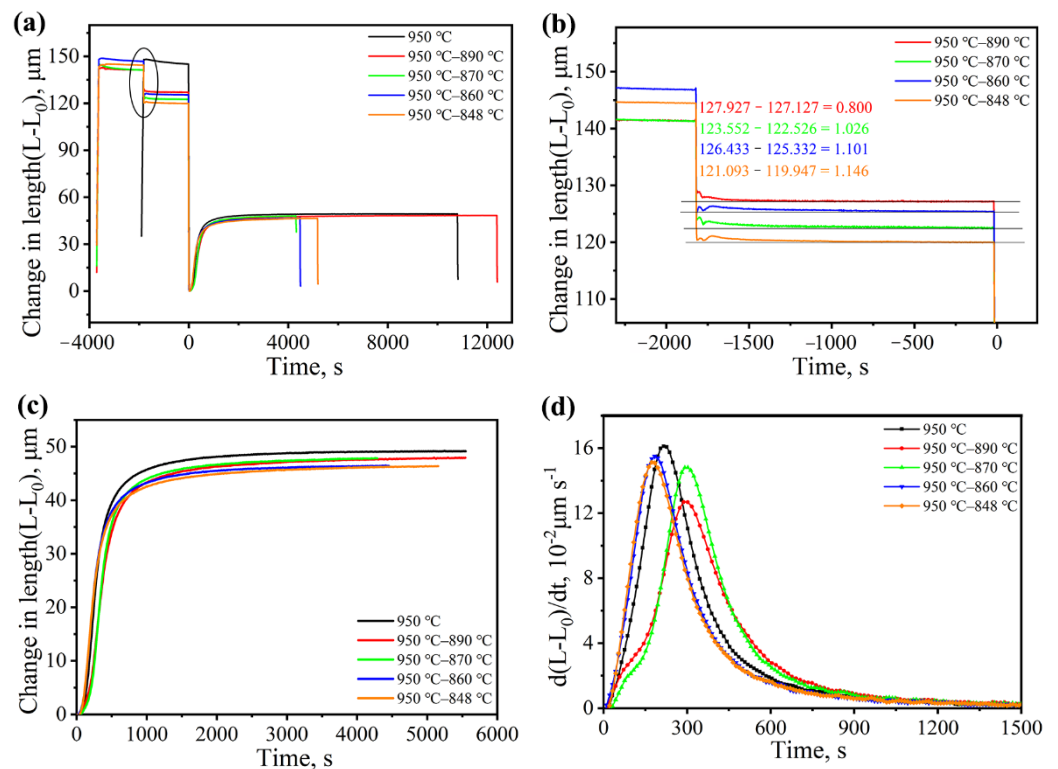


Figure 5. (a) Time–expansion curves at different temperatures; (b) changes in expansion amount under different processes; (c) isothermal curves of different processes; and (d) bainite transformation rates under different heat treatment process.

3.3. Characterization of the Second Phase

Specimens with different treatments are observed, and the SEM images are shown in Figure 6. It can be seen that the microstructure obtained by different high temperature treatment is composed of bainitic ferrite (BF) and retained austenite (RA). Film-like retained austenite (F-RA) is distributed between bainitic ferrite laths and blocky retained austenite (B-RA) is distributed among bainitic sheaves with different directions. From Figure 6b,c, it can be seen that most of the bainitic ferrite laths penetrate throughout the parent austenite grains with relatively regular distribution and single direction. In Figure 6d,e, the distribution direction of bainitic ferrite laths becomes complicated and the number of bainitic ferrite laths penetrating throughout the parent austenite grains is reduced. This indicates that the nucleation sites of bainite ferrite increase in the 950 °C–860 °C and 950 °C–848 °C treated specimens, and bainite ferrite laths in the same direction may originate from different nucleation sites, accelerating phase transformation rates.

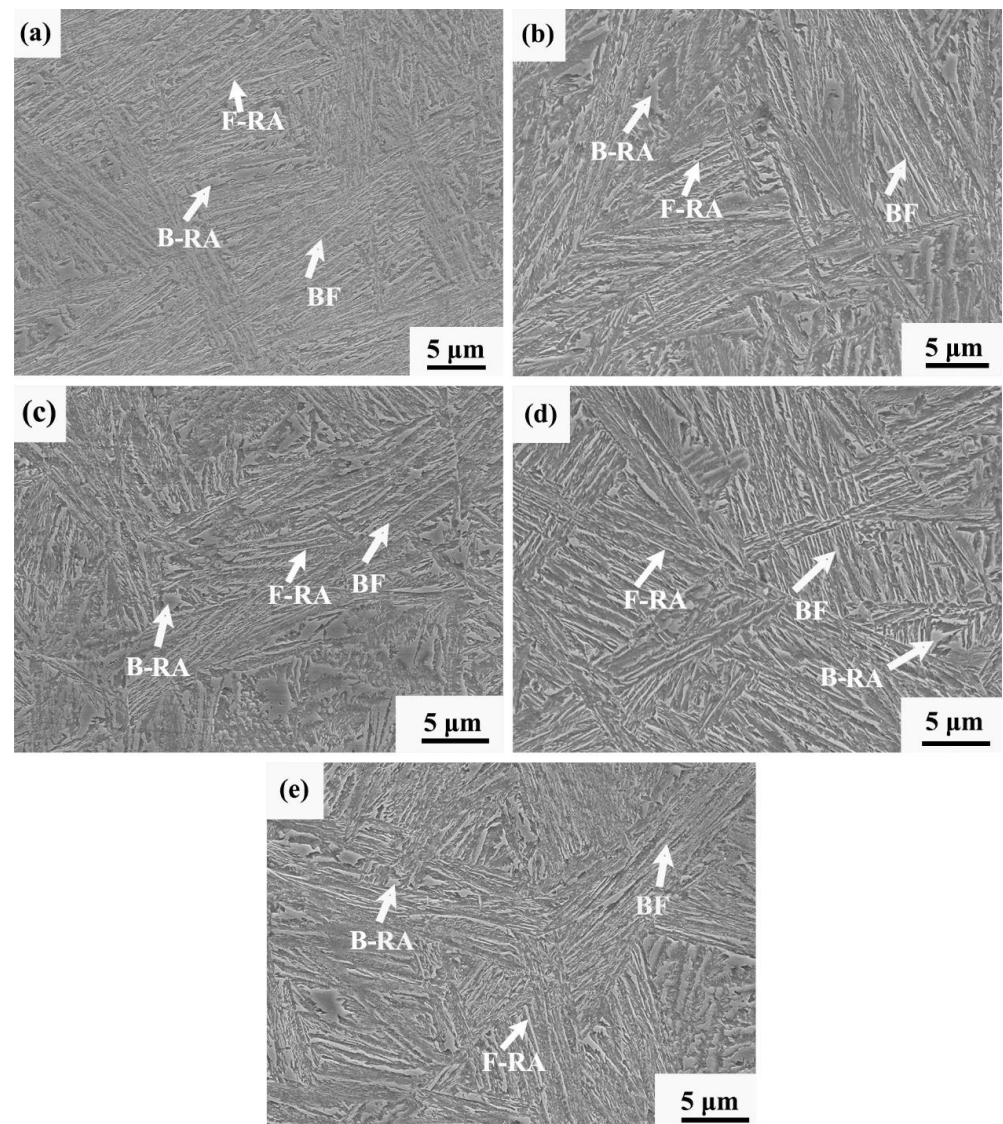


Figure 6. SEM micrographs of specimens with different heat treatment processes. (a) 950 °C; (b) 950 °C–890 °C; (c) 950 °C–870 °C; (d) 950 °C–860 °C; and (e) 950 °C–848 °C. (BF: bainitic ferrite; F-RA: film retained austenite; B-RA: blocky retained austenite).

Energy spectral analysis of the microstructure for specimens treated at 950 °C–870 °C and 950 °C–848 °C revealed carbide precipitation, as shown in Figure 7. Precipitation of V is observed, as shown in the inset image. The TEM characterization was carried out to further observe the microstructure, morphology, and volume fraction of V precipitation.

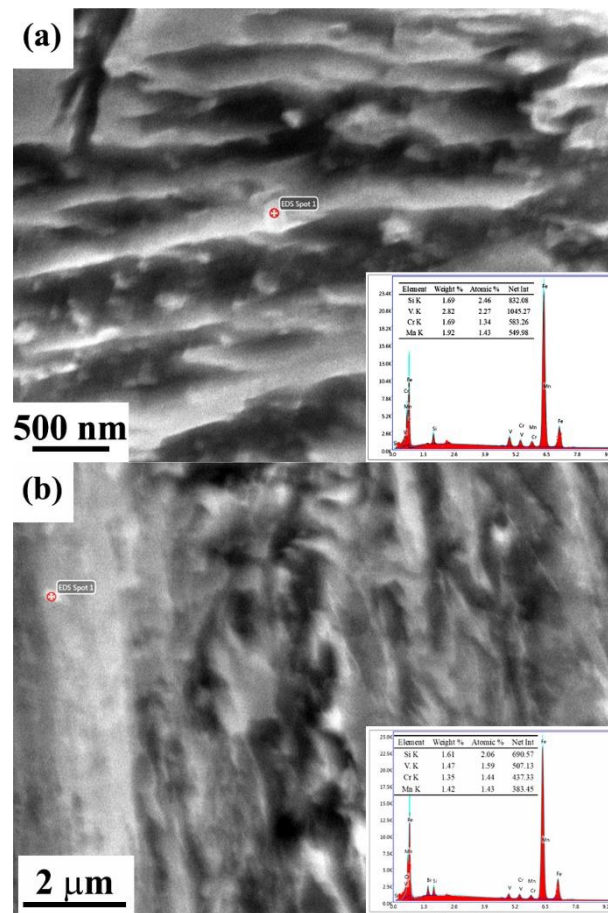


Figure 7. EDS analysis of specimen treated at 950 °C–870 °C and 950 °C–848 °C (a,b).

Figure 8 shows the TEM microstructures of three typical specimens with single- and two-step isothermal treatments. The TEM microstructure of all specimens consists of bainitic ferrite laths (bright white) and film-like retained austenite (dark gray). Bainite ferrite laths with high dislocation density are parallel to each other. The film-like retained austenite is mainly distributed among the bainitic ferrite laths. Figure 8b, d, and f are TEM images at high magnifications in the three specimens. Black diamond-shaped or ellipsoidal VC carbides with a size of about 30 nm are found in all three specimens. EDS point scans are performed in the specimens of 950 °C–848 °C and the preparations are initially identified as VC.

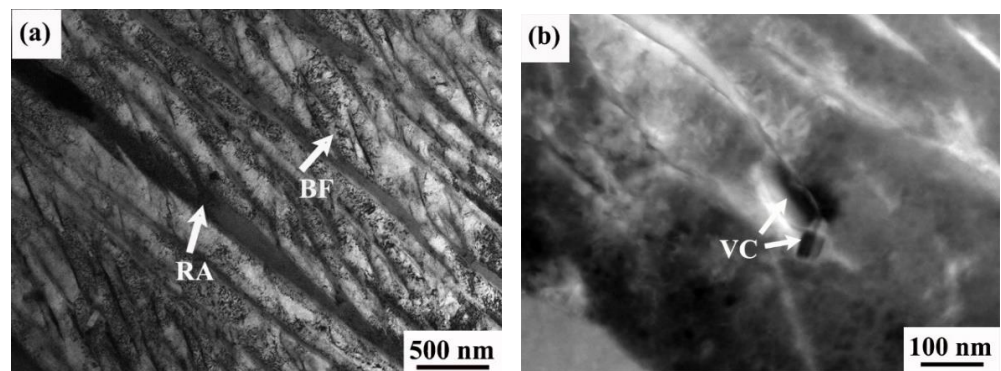


Figure 8. Cont.

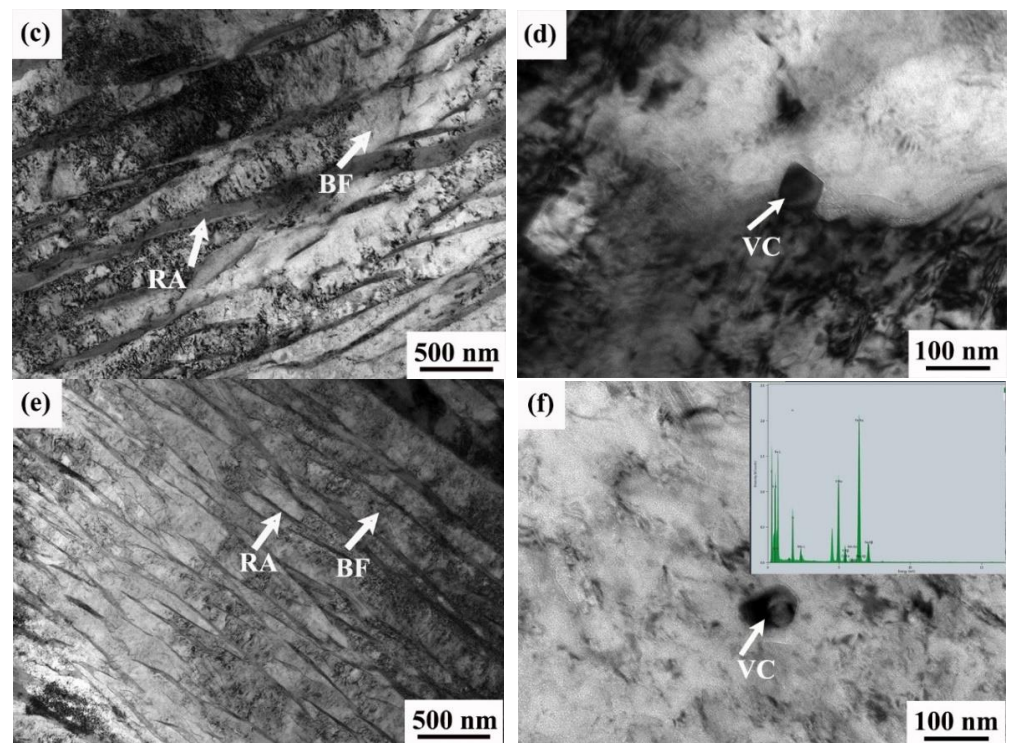


Figure 8. TEM micrographs of specimens with different heat treatment processes. (a,b) 950 °C; (c,d) 950 °C–870 °C; and (e,f) 950 °C–848 °C.

Figure 9 shows the energy spectrum analysis of samples with different heat treatment under TEM. It can be seen that as the austenitizing temperature decreases from 950 °C to 848 °C, the V precipitations become more and more, which is consistent with the results of Thermo-Calc simulation. Figure 9d shows the high magnification scan images of the specimens treated with 950 °C–870 °C. It is found that C and V elements are aggregated, and the precipitations are determined as C- and V-rich particles. Figure 10 is a high magnification TEM image of specimens after treatment at 950 °C–848 °C. Figure 10b is a high-resolution image of Figure 10a. The diffraction spots are obtained by Fourier transformation, and compared to the PDF card of standard VC precipitations. It is determined that the diffraction spot is VC, i.e., the precipitation is a VC particle.

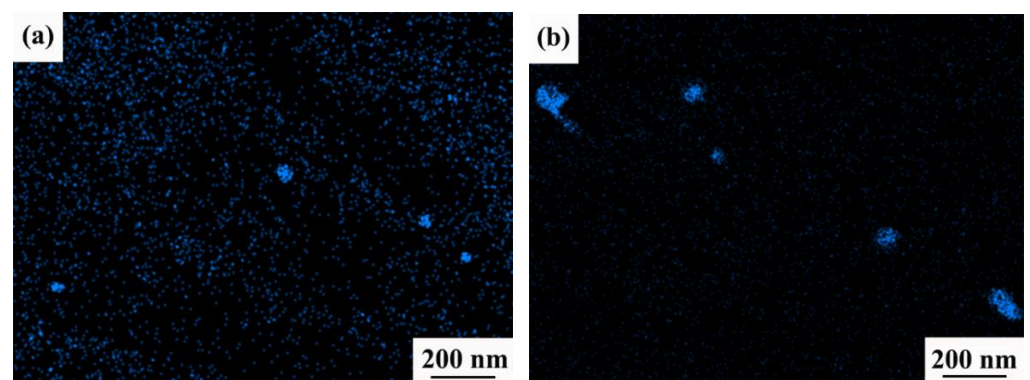


Figure 9. Cont.

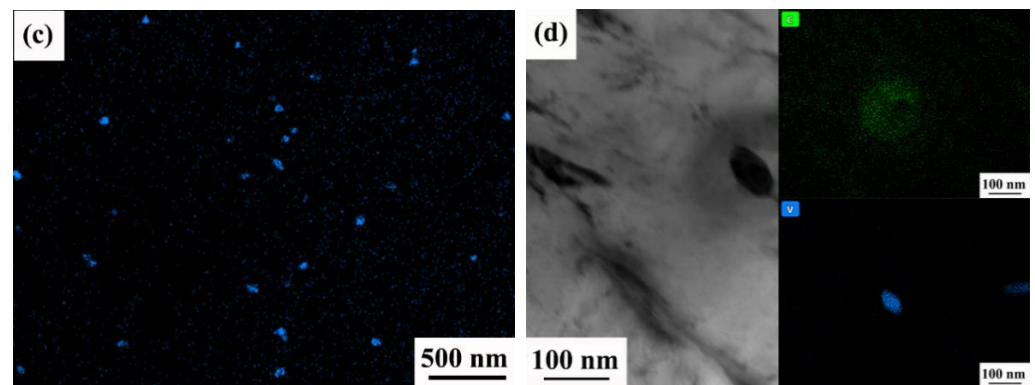


Figure 9. TEM map scanning images of different heat treatment processes (a,d) 950 °C; (b) 950 °C–870 °C; and (c) 950 °C–848 °C.

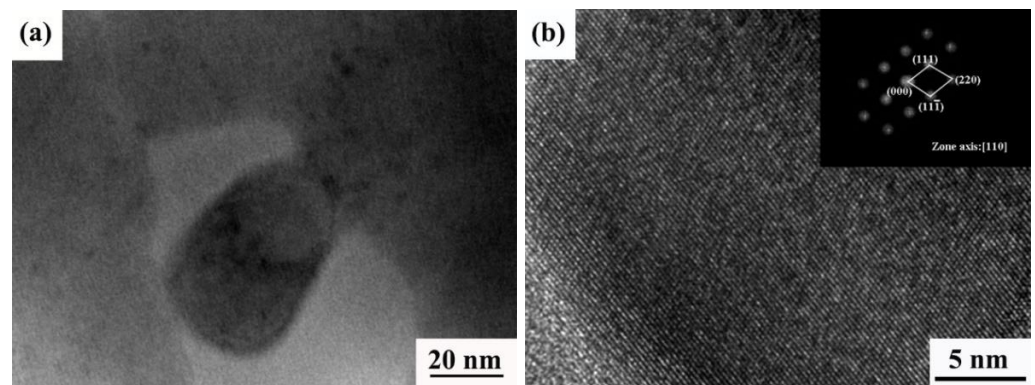


Figure 10. (a) High magnification TEM image of 950–848 process; (b) High resolution micrographs image of 950 °C–848 °C process.

3.4. Mechanical Properties

The detailed mechanical properties of these three specimens are presented in Table 1. The engineering stress–strain curves are shown in Figure 11. It can be seen that the impact toughness of the tested steel under the 950 °C–870 °C treatment is the highest, reaching 72 J/cm². The tensile strength, yield strength, elongation, impact toughness, and hardness of the steel subjected to 950 °C–848 °C treatment were 1579 MPa, 1108 MPa, 15.9 %, 50.5 J/cm², and 46.5 HRC, respectively. Compared with the specimens treated at 950 °C–870 °C with a lower amount of VC precipitations, the strength, hardness, and elongation of the specimens treated at 950 °C–848 °C were slightly increased and the impact toughness was reduced. In general, the addition of a certain amount of VC precipitations improves the comprehensive mechanical properties of the tested steel.

Table 1. Mechanical properties of the test steel under different heat treatment process.

Thermal Treatment Regime / °C	UTS, MPa	YS, MPa	EL, %	UE, %	a _{KU} , J/cm ²	Hardness, HRC
950	1575	1103	14.1	6.9	58	45.8
950–870	1562	1081	12.6	6.6	72	45.6
950–848	1579	1108	15.9	7.5	50	46.5

Note: UTS—Ultimate tensile strength; YS—Yield strength; EL—Total elongation; UE—Uniform elongation; a_{KU}: impact toughness.

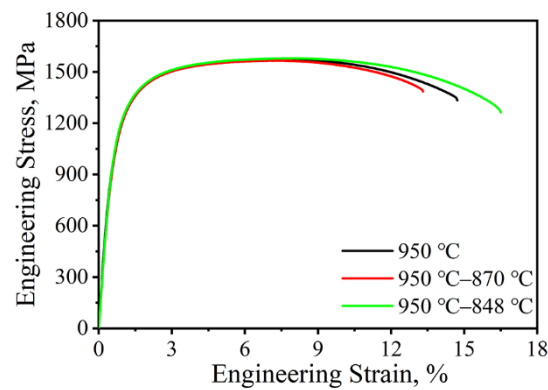


Figure 11. Engineering stress–strain curves of tested steel under different heat treatment processes.

4. Discussion

4.1. Transformation Acceleration Mechanisms

It can be seen from Figure 5 that the second-step isothermal temperature can affect bainite transformation when the second-step isothermal treatment is introduced at the high-temperature region. As mentioned in Section 3.2, the second-step of isothermal temperature are controlled in the lower temperature range of the intercritical region, accelerating the bainite transformation. However, it is worth noting that high-temperature of second-step isothermal treatment is disadvantage to accelerate bainitic transformation. The promotion or inhibition of bainitic transformation may be related to carbon segregation at parent austenite grain boundaries. Abe et al. [24] performed a two-step heat treatment similar to the two-step isothermal treatment in this study, i.e., the samples were austenitized at 1100 °C, followed by isothermal holding times of 10–1000 s at 800–1000 °C, and, finally, the specimen was cooled to room temperature. They demonstrate that the intercritical annealing treatment resulted in carbon segregation at parent austenite grain boundaries compared to the samples cooled directly from the austenitization temperature. Abe et al. [24] concluded that the degree of the carbon segregation during intercritical annealing treatment increases with increasing of holding time and decreasing intercritical annealing temperature. Kang et al. [25] reported the distribution of carbon atoms near parent austenite grain boundaries in several high carbon steels after isothermal holding at 300 °C for a short time. They observed that isothermal holding brought about the carbon enrichment at the parent austenite grain boundaries and the formation of carbon-depleted regions near the parent austenite grain boundaries (200 nm away from the grain boundary). Zhang et al. [26] obtained similar results in another study. Kang et al. [23] indicated that the formation of carbon-rich and carbon-poor regions during the isothermal treatment is a result of dislocation and grain boundary related stress fields. The formation of carbon-rich and carbon-poor regions are called as pre-bainite phenomenon. Low carbon regions favor bainite nucleation. The driving force for bainite formation increases as the carbon concentration in the austenitic matrix decreases. Aaronson et al. [27] suggested that carbon-depleted regions near parent austenite grain boundaries exist only for a limited time, until the chemical potential of carbon atoms in the austenite grain boundaries is the same as that in the matrix. Aaronson [27] proposed that a wide range of carbon-rich region and corresponding carbon-poor regions exist during isothermal holding, indicating that austenite is decomposed into phases with low-carbon solubility, such as ferrite.

In this study, the microstructure of the 950 °C–860 °C and 950 °C–848 °C treated specimens do not show any ferrite (Figures 6 and 8). Therefore, the acceleration of the kinetics of bainitic transformation due to the formation of a ferrite/austenite interfaces can be ignored. However, the second-step isothermal temperatures of 860 °C and 848 °C are in the intercritical temperature range. There is a driving force for ferrite formation. Therefore, it can be assumed that the carbon atoms deviate towards the parent austenite grain boundaries leading to fluctuations in the carbon composition near the grain boundaries.

During the second-step isothermal treatment, these carbon fluctuations can lead to the formation of stable ferrite nuclei. The increase in the number of stable ferrite nuclei with bcc structure increases the density of bainitic nucleation sites. The results of Sun et al. show that decreases in activation energy for bainite nucleation at vanadium carbide/austenite interfaces lead to a favorable acceleration of bainitic formation kinetics [13]. In this study a large number of VC particles precipitated during the second-step isothermal treatment increase abundant VC/austenite interfaces, which provides preferential nucleation position for bainitic ferrite. These two factors combine to accelerate the bainite transformation.

For 950 °C–890 °C and 950 °C–870 °C treated specimens, the second-step isothermal temperatures are in the austenitization range. There is no driving force for the ferrite formation. Moreover, the number of VC particles precipitated during the second-step isothermal treatment is small. Especially, the number of VC particles precipitated at 890 °C is extremely small (Figure 3b). Therefore, the effect of accelerating bainitic transformation rate of the two specimens is not obvious. It has also been reported that the reduction in bainite transformation rate is also related to the reduction in the diffusion rate of carbon atoms in austenite due to solid solution of V atoms in the matrix at high temperatures [28]. In addition, V, as a strong carbide forming element, tends to form atomic clusters in the supercooled austenite, making the migration of carbon atoms difficult. As a result, the bainite transformation rate is reduced.

4.2. Effect of Second-Phase Precipitation on Phase Composition

XRD analysis of all the DIL specimens after high-temperature two-step isothermal treatment was performed to study the phase composition, as shown in Figure 12. There are only ferrite and retained austenite according to XRD curves, therefore, the volume fraction of retained austenite can be calculated by using the formula in [29]. The volume fractions of the retained austenite are listed in Table 2. As the isothermal temperature decreases from 950 °C to 848 °C, the volume fraction of retained austenite firstly increases and then decreases. The reasons for the evolution of retained austenite volume fraction are as follows. When the specimen is isothermal at 950 °C, a large number of V atoms are dissolved in the matrix, while the effect of VC particles on grain boundary pinning is not obvious. Therefore, the transformation of austenite to bainitic ferrite is easy, resulting in the decrease in volume fraction of retained austenite. When the isothermal temperature decreases, the precipitation of VC particles increases. The formation of VC particles in the microstructure reduces the carbon content in the undercooled austenite and makes the undercooled austenite unstable. Therefore, the undercooled austenite is easy to transform into bainitic ferrite. However, at the same time, the degree of grain boundary pinning caused by more VC particles of the low-temperature isothermal specimen is relatively higher than that of the high-temperature isothermal specimen. Consequently, the transformation of supercooled austenite to bainitic ferrite is difficult. The latter is the crucial factor in the above mentioned two factors affecting the transformation fraction of undercooled austenite, eventually leading to an increase in the volume fraction of retained austenite. The amount of VC particles increases with the further decrease of isothermal temperature; thus, the carbon content in retained austenite continues to decrease. Moreover, the pinning effect of small VC particle is relatively smaller. As a result, the undercooled austenite is easy to transform to bainitic ferrite, and the volume fraction of retained austenite decreases.

Table 2. The volume fraction of the retained austenite of the samples after high-temperature two-step isothermal treatment.

Temperature/°C	950	950–890	950–870	950–860	950–848
V _{RA} /%	13.3	18.6	15.1	14.9	13.8

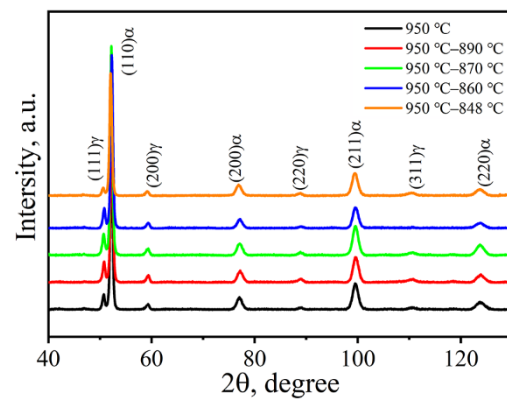


Figure 12. XRD patterns of the specimens after high-temperature two-step isothermal treatment.

4.3. Characteristics of Orientation and Substructure

EBSD analysis was carried out to further analyze the difference in the misorientation angle of the specimens after different heat treatment processes. Inverse pole figure (IPF) and misorientation angle distributions of the specimens are shown in Figure 13. The proportion of the misorientation angle less than 5° of the 950°C – 848°C treated specimen is large. The low-angle grain boundaries with very small misorientation angles ($<5^\circ$) are regarded as substructures existing in the grains, which is beneficial to the improvement of strength [30,31]. In contrast, the proportion of low-angle grain boundaries of 950°C – 870°C treated specimen is small, while that of high-angle grain boundaries is large. Studies have shown that high-angle grain boundaries between bainite can hinder crack propagation or change crack propagation direction, which can improve the toughness of specimens [32,33]. Therefore, the 950°C – 870°C treated specimen exhibits high impact toughness.

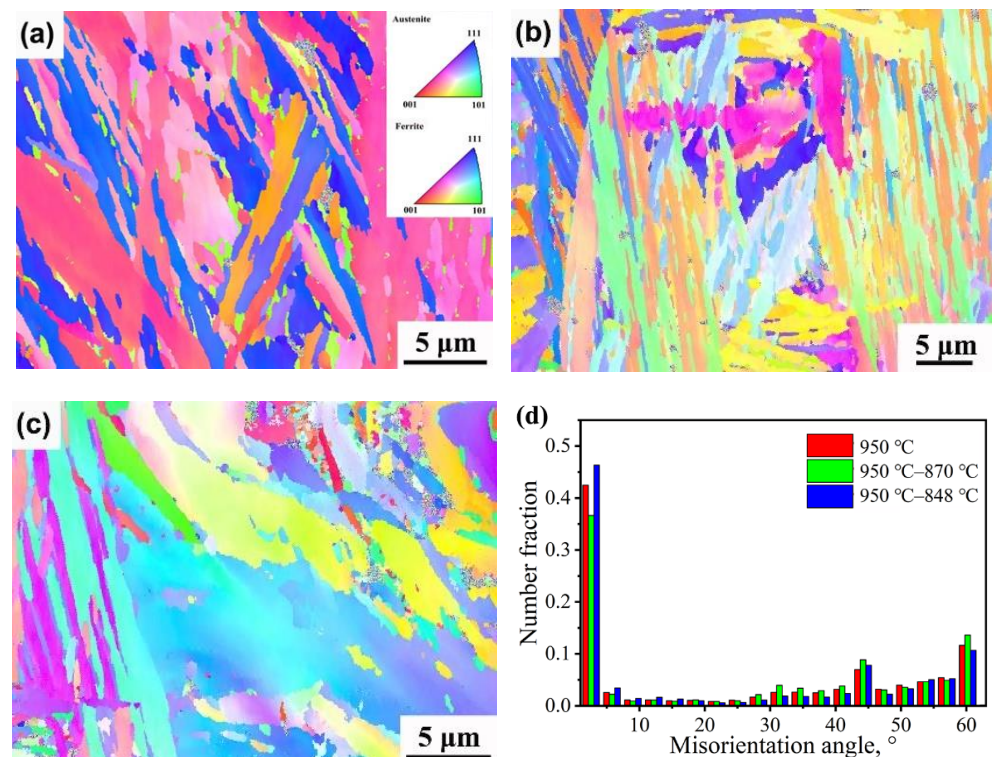


Figure 13. IPF maps ((a) 950°C ; (b) 950°C – 870°C ; and (c) 950°C – 848°C) and misorientation angle distributions (d) of the samples after high-temperature two-step isothermal processes.

5. Conclusions

Microalloyed Fe-0.397C-1.527Mn-1.525Si-1.087Cr-0.31Mo-0.15V medium-carbon bainite steel was investigated in this study. Different amounts of VC particles were introduced in the second stage of the high temperature isothermal treatment before the bainitic austempering. Their effect on the kinetics of bainite transformation, as well as on the microstructure and mechanical properties, was investigated. The main conclusions are as follows:

1. The bainite transformation kinetics is accelerated when the isothermal temperature of the second stage is in the intercritical annealing range, i.e., at 860 °C and 848 °C. No ferrite is formed in this range. However, there is a driving force to form ferrite nuclei, which could serve as bainite nucleation sites to accelerate bainite transformation. In addition, numbers of VC particles precipitate at these temperatures. The increased phase interfaces of VC particles also provide as preferential nucleation sites for bainite transformation, synergistically accelerating the bainite transformation;
2. The microstructure of the high-temperature two-step isothermal treated specimens mainly consists of bainite ferrite and residual austenite, and also contains VC precipitations. As the temperature decreases from 950 °C to 848 °C, the number of VC precipitations increases and the volume fraction of residual austenite tends to increase and then decrease;
3. The specimens treated at 950–870 °C show high impact toughness. These specimens are dominated by high angle grain boundaries, which can hinder or change the direction of crack expansion. The strength of the specimens treated at 950–848 °C is improved, which is related to the presence of large number of sub-structures (dislocations, stacking fault, and sub-grain.) within the grains.

Author Contributions: Conceptualization, X.L., B.L. and Z.Y.; methodology, D.Y. and Z.L.; data collection, D.S. and D.Y.; data analysis, B.L., D.Y. and Z.L.; writing—original draft preparation, B.L. and X.L.; writing—review and editing, D.S., X.L. and Z.Y. All authors have read and agreed to the published version of the manuscript.

Funding: The authors acknowledge financial support from the National Key R&D Program of China (2021YFB3703500), the National Natural Science Foundation of China (No. 52001275), the Natural Science Foundation of Hebei Province (E2020203084), and the Youth Talent Projects of Colleges in Hebei Province (BJ2020021).

Institutional Review Board Statement: Not applicable.

Informed Consent Statement: Not applicable.

Data Availability Statement: Not applicable.

Conflicts of Interest: The authors declare that they have no known competing financial interests or personal relationships that could have appeared to influence the work reported in this paper.

References

1. Foster, D.; Paladugu, M.; Hughes, J.; Kapousidou, M.; Barcellini, C.; Daisenberger, D.; Jimenez-Melero, E. Comparative micromechanics assessment of high-carbon martensite/bainite bearing steel microstructures using in-situ synchrotron X-ray diffraction. *Materialia* **2020**, *14*, 100948. [[CrossRef](#)]
2. Kumar, A.; Makineni, S.K.; Dutta, A.; Goulas, C.; Steenbergen, M.; Petrov, R.H.; Sietsma, J. Design of high-strength and damage-resistant carbide-free fine bainitic steels for railway crossing applications. *Mater. Sci. Eng. A* **2019**, *759*, 210–223. [[CrossRef](#)]
3. Haiko, O.; Kaikkonen, P.; Somani, M.; Valtonen, K.; Kmi, J. Characteristics of carbide-free medium-carbon bainitic steels in high-stress abrasive wear conditions. *Wear* **2020**, *456–457*, 203386. [[CrossRef](#)]
4. Zhu, K.Y.; Mager, C.; Huang, M.X. Effect of substitution of Si by Al on the microstructure and mechanical properties of bainitic transformation-induced plasticity steels. *J. Mater. Sci. Technol.* **2017**, *33*, 1475–1486. [[CrossRef](#)]
5. Soliman, M.; Palkowski, H. Development of the low temperature bainite. *Arch. Civ. Mech. Eng.* **2016**, *16*, 403–412. [[CrossRef](#)]
6. Catteau, S.D.; van Landeghem, H.P.; Teixeira, J.; Dulcy, J.; Dehmas, M.; Denis, S.; Redjaïmia, A.; Courteaux, M. Carbon and nitrogen effects on microstructure and kinetics associated with bainitic transformation in a low-alloyed-steel. *J. Alloys Compd.* **2016**, *65*, 832–838. [[CrossRef](#)]

7. Zhao, X.J.; Yang, Z.N.; Zhang, F.C.; Long, X.Y.; Chen, C. Acceleration of bainitic transformation by introducing AlN in medium carbon steel. *Mater. Sci. Technol.* **2019**, *35*, 147. [[CrossRef](#)]
8. Ravi, A.M.; Kumar, A.; Herbig, M.; Sietsma, J.; Santofimia, M.J. Impact of austenite grain boundaries and ferrite nucleation on bainite formation in steels. *Acta Mater.* **2020**, *188*, 424–434. [[CrossRef](#)]
9. Hu, H.J.; Tian, J.Y.; Xu, G.; Zurob, H.S. New insights into the effects of deformation below-M_s on isothermal kinetics of bainitic transformation. *J. Mater. Res. Technol.* **2020**, *9*, 15750–15758. [[CrossRef](#)]
10. Lagneborg, R.; Siwecki, T.; Zajac, S.; Hutchinson, B. The role of vanadium in microalloyed steels, *Scand. J. Met.* **1999**, *28*, 186–241.
11. Escobar, J.D.; Faria, G.A.; Maia, E.L.; Oliveirad, J.P.; Bollef, T.; Seilsef, S.; Meia, P.R.; Ramirez, A.J. Fundamentals of isothermal austenite reversion in a Ti-stabilized 12Cr–6 Ni–2Mo super martensitic stainless steel: Thermodynamics versus experimental assessment. *Acta Mater.* **2019**, *174*, 246–259. [[CrossRef](#)]
12. Escobar, J.D.; Oliveira, J.P.; Salvador, C.A.F.; Tschiptschina, A.P.; Meid, P.R.; Ramirez, A.J. Double-step inter-critical tempering of a supermartensitic stainless steel: Evolution of hardness, microstructure and elemental partitioning. *Mater. Character* **2019**, *158*, 109994. [[CrossRef](#)]
13. Garcia, C.; Cornide, J.; Capdevila, C. Influence of V Precipitates on acicular ferrite transformation Part 2: Transformation kinetics. *ISIJ Int.* **2008**, *48*, 1276–1279. [[CrossRef](#)]
14. Yong, Q.L. *The Second Phase in Iron and Steel*; Metallurgical Industry Press: 2006, Beijing, China.
15. Sun, D.; Liu, C.; Long, X.; Zhao, X.; Li, Y.; Lv, B.; Zhang, F.; Yang, Z. Effect of introduced vanadium carbide at the bay region on bainite transformation, microstructure and mechanical properties of high-carbon and high-silicon steel. *Mater. Sci. Eng.* **2021**, *811*, 141055. [[CrossRef](#)]
16. Wang, Y.; Gui, M.; Zhou, Y.; Ma, D.S.; Dong, H. Effect of V and N microalloying on properties of high carbon steel 82B. *Trans. Mater. Heat Treat.* **2011**, *32*, 82–86. [[CrossRef](#)]
17. Nafsi, S.; Shalchi Amirkhiz, B.; Fazeli, F.; Arafn, M.; Glodowski, R.; Collins, L. Effect of vanadium addition on the strength of API X100 linepipe steel. *ISIJ Int.* **2016**, *56*, 154–160. [[CrossRef](#)]
18. Wang, Z.H.; Hui, W.J.; Yong, Z.C.; Zhao, X.L. Effect of vanadium on microstructure and mechanical properties of bainitic forging steel. *Mater. Sci. Eng.* **2020**, *771*, 138653. [[CrossRef](#)]
19. Karmakar, A.; Mukherjee, S.; Kundu, S.; Srivastava, D.; Mitra, R. Effect of composition and isothermal holding temperature on the precipitation hardening in Vanadium-microalloyed steels. *Mater. Character* **2017**, *132*, 31–40. [[CrossRef](#)]
20. Siwecki, T.; Eliasson, J.; Lagneborg, R.; Hutchinson, B. Vanadium microalloyed bainitic hot strip steels. *ISIJ Int.* **2010**, *50*, 760–767. [[CrossRef](#)]
21. Nafisi, S.; Arafin, M.; Glodowski, R.; Collins, L.; Szpunar, J. Impact of vanadium addition on API X100 steel. *ISIJ Int.* **2010**, *10*, 2404–2410. [[CrossRef](#)]
22. Garmeh, B.; Kasiri-Asgarani, M.; Amini, K.; Ghayour, H.; Bakhsheshi-Rad, H.R. Effect of Vanadium and Rare Earth on the Structure, Phase Transformation Kinetics and Mechanical Properties of Carbide-Free Bainitic Steel Containing Silicon. *Appl. Sci.* **2022**, *12*, 1668. [[CrossRef](#)]
23. Xu, Z. *Thermodynamics of Metal Materials*. Science Press: Beijing, China, 1981.
24. Abe, T.; Tsukada, K.; Tagawa, H.; Kozasu, I. Grain boundary segregation behaviour of phosphorus and carbon under equilibrium and non-equilibrium conditions in austenitic region of steels. *ISIJ Int.* **1990**, *30*, 444–450. [[CrossRef](#)]
25. Kang, M.K.; Yang, Y.Q.; Wei, Q.M.; Yang, Q.M.; Meng, X.K. On the prebainitic phenomenon in some alloys. *Metal. Mater. Trans.* **1994**, *25*, 1941–1946. [[CrossRef](#)]
26. Zhang, M.X.; Kelly, P. Determination of carbon content in bainitic ferrite and carbon distribution in austenite by using CBKLDLP. *Mater. Character.* **1998**, *40*, 159–168. [[CrossRef](#)]
27. Aaronson, H.; Hirth, J. On the thermodynamics of precipitate plate formation by shear above t₀ assisted by solute adsorption effects. *Scr. Metall. Mater.* **1995**, *33*, 347–353. [[CrossRef](#)]
28. Li, Z.; Zhang, X.; Mi, Z.; Li, H. Effect of alloying element V on the microstructure and properties of high carbon chromium bearing steel. *Trans. Mater Heat Treat.* **2015**, *36*, 125–132. [[CrossRef](#)]
29. De, A.K.; Murdock, D.C.; Mataya, M.C.; Speer, J.G.; Matlock, D.K. Quantitative measurement of deformation-induced martensite in 304 stainless steel by X-ray diffraction. *Scr. Mater.* **2004**, *50*, 1445–1449. [[CrossRef](#)]
30. Rauch, G. Dislocation structure misorientations measured with an automated electron diffraction pattern indexing tool. *Mater. Sci. Eng.* **2007**, *462*, 402–406. [[CrossRef](#)]
31. Wu, P.C.; Chang, C.P.; Kao, P.W. The distribution of dislocation walls in the early processing stage of equal channel angular extrusion. *Mater. Sci. Eng.* **2004**, *374*, 196–203. [[CrossRef](#)]
32. Bevis, H.; Jacek, K.; Gregory, S.; Rohrer, H.B. Heat affected zone microstructures and their influence on toughness in two microalloyed HSLA steels. *Acta Mater.* **2015**, *97*, 380–391. [[CrossRef](#)]
33. Brozzo, P.; Buzzichelli, G.; Mascanzoni, A. Microstructure and cleavage resistance of low-carbon bainitic steels. *Met. Sci.* **1977**, *11*, 123–130. [[CrossRef](#)]